12-2015

Modulation of Valve Interstitial Cell Function through Cell Shape and Phenotype

Atefeh Razavi
University of Arkansas, Fayetteville

Modulation of Valve Interstitial Cell Function through Cell Shape and Phenotype

A thesis submitted in partial fulfillment
of the requirements for the degree of
Master of Science in Biomedical Engineering

by

Atefeh Razavi
Yazd University
Bachelor of Science in Mechanical Engineering, 2005
Isfahan University of Technology
Master of Science in Mechanical Engineering, 2009

December 2015
University of Arkansas

This thesis is approved for recommendation to the Graduate Council.

_____
Dr. Kartik Balachandran
Thesis Advisor

_____
Dr. Timothy Muldoon
Committee Member

_____
Dr. Jeffrey Wolchok
Committee Member

ABSTRACT

The aortic valve is a highly dynamic structure responding to actively to the chemical, mechanical and physical cues of the valve microenvironment. Valve interstitial cells are dispersed throughout the valve tissue and play an important role in maintaining the integrity and optimum function of the valve. They are a heterogeneous population composed of various phenotype. These phenotypes have specific functions characteristic of valve physiological and pathological conditions. The effect of mechanical loading and chemical modulators on the behavior of the valve interstitial cells have largely been studied. However the role of valve interstitial cell shape as an intrinsic physical cue on cell behavior has not been considered yet. Based on the actively responsive nature of the valve interstitial cells and the evidence of the relationship between cellular shape and behavior for the other types of cells, we decided to investigate the effects of valve interstitial cells shape on the contractile function and phenotype modulation. Various cell shapes were designed by constraining the cells into different line/pattern widths (10μm, 20μm, 40μm, 60μm, and 80μm) using soft lithographic techniques. Cells were aligned into the lines exhibiting varied cytoskeletal organizations. Orientation of the actin filaments significantly decreased with increasing the pattern width. A similar trend was observed for the cell aspect ratio and nuclear eccentricity. Contractile function of the cells was examined utilizing a custom valavular thin film assay. All the films of the tissue construct responded to the vasoconstrictive and vasodilatory drugs. Cellular maximum contraction did not reveal any specific trend while cell basal tone had some statistical variations showing the maximum value for 40μm in which cell-cell contact and cell elongation may have interacted optimally. Analysis of the contractile and activated phenotype markers was performed using western blot on vimentin, α-smooth muscle actin and smooth muscle myosin heavy chain. The expression of these proteins did not change significantly for the patterns suggesting that the cell contractility may be more correlated

to the cell shape than phenotype. In conclusion we were able to modulate valve interstitial cellular shape using soft lithographic techniques and cause alterations in cellular function. Cell phenotype may not be a regulating factor of the cell behavior as commonly measured.

ACKNOWLEDGMENTS

I would like to take this opportunity to express my gratitude to everyone who has supported, assisted, and encouraged me through my graduate studies.

I would like to thank Dr. Kartik Balachandran, my advisor and director of the Mechanobiology and Soft Materials lab who enthusiastically answered all my questions, and patiently helped and advised me throughout my master program. His useful guidance and critique will help me to become a better researcher.

Dr. Timothy Muldoon, Dr. Jeffrey Wolchok and Dr. David Zaharoff who generously let me use their lab facilities.

Former and current students in the laboratory. I would specially like to thank Prashanth Balaji and Jessica Morales for their generosity in helping me throughout the experiments.

Faculty and staff of Biomedical Engineering department.

I also would like to thank Sruthi Ravindranathan for all of her continuous help and support and real friendship since I started school here.

Finally I would like to thank my mom, my dad and my brothers for their extreme love and support in every step of my life.

TABLE OF CONTENTS

CHAPTER ONE 1
INTRODUCTION 1
1-1 Aortic Valve Anatomy 2
1-2 Aortic Valve Cellular Phenotypes 3
1-3 Multiscale Study of Mechanobiology of Healthy and Diseased Aortic Valve 5
1-4 Tissue-Level Studies 6
1-5 Cell-Level Studies 7
1-6 Chemical Stimulation Studies at Cell Level 7
1-7 Mechanical Stimulation Studies at Cell Level 9
1-8 Cell Shape on Other Cell Types 9
1-9 Motivation for Thesis 13
1-10 Hypothesis and Objectives 13
CHAPTER TWO 15
MATERIALS AND METHODS 15
2-1 Cell Isolation 15
2-2 Mask Design and Soft Lithography 15
2-3 Micro-contact Printing 18
2-3-1 Cell Substrate Preparation for Protein Blotting 18
2-3-2 Cell Substrate Preparation for Valve Thin Film Assay 20
2-4 Valve Thin Film Assay 21
2-5 Fluorescent staining for cell and nuclear architecture analysis 22
2-6 Western Blotting 23
2-7 Statistical Analysis 24
CHAPTER THREE 25
RESULTS 25
3-1 *In vitro* model for altered cell shape 25
3-2 Role of cell shape on valve interstitial cell architecture 25
3-3 Role of cell shape on valve interstitial cell function 27
3-4 Role of cell shape on valve interstitial cell phenotype 30
Table 3.1 Antibodies used to describe activated and smooth muscle cell phenotype 31
CHAPTER FOUR 33

DISCUSSION **33**
CHAPTER FIVE **37**
Conclusions and Future Directions **37**
REFERENCE **39**
APPENDIX **44**
MATLAB CODE **44**

CHAPTER ONE

INTRODUCTION

The aortic valve is a complex structure functioning in a harsh dynamic environment ensuring unidirectional blood flow from the left ventricle into the body. It opens and closes over 2 billion times over an average lifespan of 70 years. Previously, it was assumed to perform passively as a result of just transvalvular pressure differences on the leaflets and contraction or relaxation of the myocardium. However recent studies show that sophisticated mechanisms are involved in aortic valve function affecting valvulogenesis in embryonic development [2], valve growth and adaptation in adulthood [3, 4], and valve degeneration and dysfunction in the diseased state [5]. These mechanisms take place at the molecular, cellular and tissue levels in response to various stimulations via signaling pathways, such as inflammation, and ECM remodeling leading to a diseased and dysfunctional state. Heart valve diseases account for 23000 deaths annually in the United States, with calcific aortic valve disease (CAVD) being the most prevalent [6].

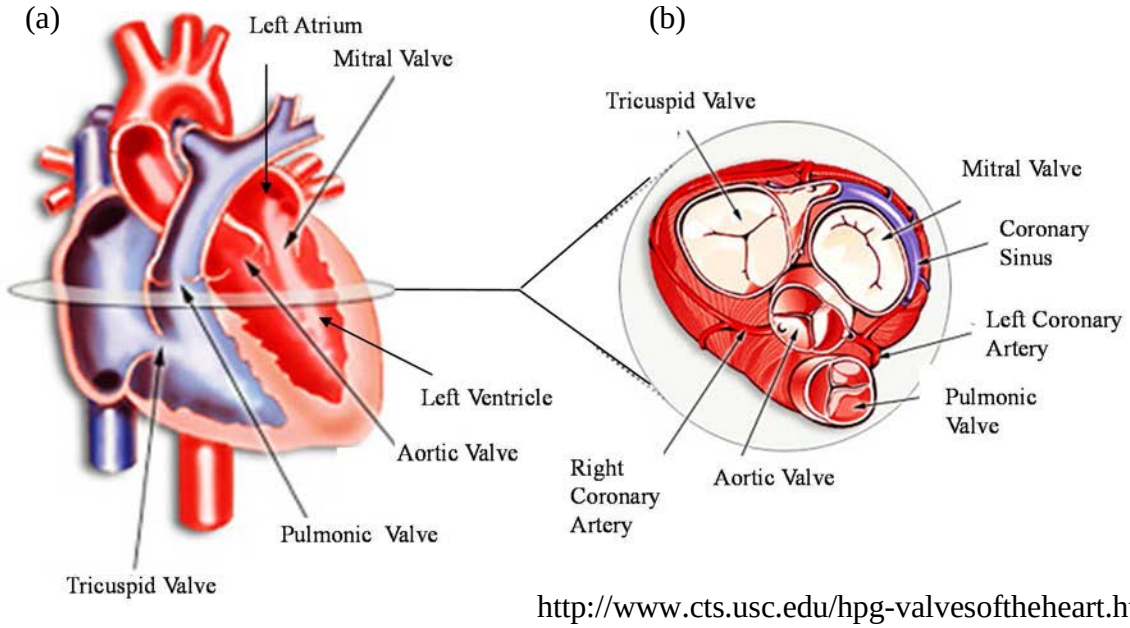

http://www.cts.usc.edu/hpg-valvesoftheheart.html

Fig 1.1. Anatomical illustration of the heart showing valve chambers and leaflets, a) longitudinal section b) axial section

Therapeutic methods for CAVD currently include heart valve replacement through open heart surgery or the application of a transcatheter aortic valve as a non-invasive method. Patients with severe aortic stenosis who do not receive valve replacement have a mortality rate of 37% at 1 year after the beginning of the symptoms [7]. There is currently no medication or pharmaceutical treatment for CAVD. Understanding the role of factors including chemical modulators, mechanical stimulations and physical cues of the valve microenvironment that may contribute to the initiation and progression of the diseases and their related underlying mechanisms will help to develop new ideas to prevent the disease progression into late stages and even treatment of the disease.

The following sections include a brief summery on the morphology, healthy and diseased stages of the aortic valve and its tissue and cellular implications.

1-1 Aortic Valve Anatomy

The aortic valve has three leaflets named left coronary, non-coronary and right coronary, based on their relative position to the coronary artery ostia. As it can be seen form Fig 2 each leaflet is composed of mainly three extracellular matrix layers termed ventricularis, spongiosa, and fibrosa. These layers have distinct chemical compositions and possess heterogeneous mechanical behavior. The ventricularis is situated on the left ventricle side of the valve. It has high elastin and fibrillar collagen content and is a load bearing component. The role of the ventricularis is to facilitate elastic recoil and expansion during systole and diastole [8, 9]. The fibrosa is located on the aortic side of the valve containing a network of circumferentially arranged collagen fibers and it also acts as a tensile load bearing component providing the required leaflet coaptation to maintain valve durability [10]. The spongiosa is the central layer, coupling the ventricularis and the fibrosa and primarily composed of glycosaminoglycans (GAGs) and proteoglycans (PGs)

with a loose organization of dispersed collagen [8]. The hydrophilic PGs of the spongiosa act as a cushion and lubricate local movement and shearing between fibrosa and ventricularis layers during cyclic loading and pressurization [11].

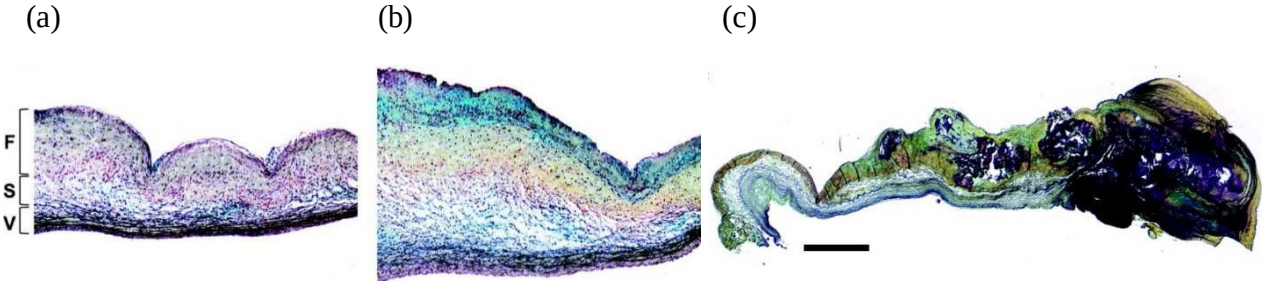

Fig 1.2. Aortic valve structure and composition A, Normal porcine aortic valve leaflet stained with Movat pentachrome, demonstrating the trilaminar structure, the collagen-rich fibrosa (F), proteoglycan-rich spongiosa (S), and elastin-containing ventricularis (V). B, Aortic valve showing early signs of valve disease, including thickening, increased matrix protein deposition (blue) and elastin fragmentation (black). C, A calcified human aortic valve leaflet demonstrating obvious maladaptive extracellular matrix (ECM) remodeling, including significant calcificatio[11] (purple)

1-2 Aortic Valve Cellular Phenotypes

There are two types of cells that reside in the aortic valve leaflet: valve endothelial cells (VECS) and valve interstitial cells (VICs). VECs lie on both surface sides of the valve and are exposed to distinct flow velocity and fluid shear stress conditions. The ventricular side VECs are under high shear stress caused by high velocity systolic outflow whereas VECs that lie on the aortic side experience the low shear stress diastolic blood flow. VECs are involved in valve homeostasis and ECM remodeling via permeability regulation [12], inflammatory responses of adhesion molecules [13]and paracrine signaling [14]. VECs and VICs are able to respond biologically to the alterations caused by mechanical stimuli via a phenomenon termed mechanotransduction. VICs lie within the body of the extracellular matrix (ECM) and exist in all three layers of the leaflet. They communicate with each other as well as with the ECM and VECs. VICs are a

heterogeneous population categorized into 5 different phenotypes [15]. These phenotypes include embryonic progenitor endothelial/mesenchymal cells, quiescent VICs (**qVICs**), activated VICs (**aVICs**), progenitor VICs (**pVICs**), and osteoblastic VICs (**obVICs**). The embryonic progenitor endothelial/mesenchymal cells undergo endothelial-to-mesenchymal transformation (Endo-MT) during embryonic valve development. The **qVICs** are observed in normal adult valve and regulate valve structure and integrity. The **aVICs** known as myofibroblasts comprise less than 5% of the total VICs, and are increased as a pathobiological response to the disease and injury through ECM remodeling, cell proliferation and migration. The pVICs are the least well defined and consist of a heterogeneous population of progenitor cells that may be important in repair. The **ObVICs** are osteoblast transdifferentiated VICs that regulate chondrogenesis and osteogenesis and promote calcification.

VICs also can exhibit smooth muscle cell phenotype (SMC) in the normal and diseased valve. In the normal valve, SMC-like VICs reside in the base of the ventricularis while in the diseased calcified valve, they have an uncharacteristic localization to the fibrosa and spongiosa [16]. All three activated, osteoblastic and SMC like cells are defined by specific markers characteristic of their phenotype. Alpha-smooth muscle actin (α-SMA) expression is recognized as a marker for aVICs. SMCs also express α-SMA as well as smooth muscle myosin heavy chain 1 and 2 that is not expressed by the activated myofibroblasts (aVICs) [10].

The osteoblastic differentiation markers of obVICs include alkalinephosphatase (ALP) [17], osteopontin (OPN) [18] , bone sialoprotein (BSP) [19, 20], bone morphogenetic proteins-2 and -4 (BMP-2 and -4) [21], as well as osteocalcin (OCN) [19, 22].

1-3 Multiscale Study of Mechanobiology of Healthy and Diseased Aortic Valve

The *in vitro* study of normal and pathological aortic valves can be categorized into the tissue and cellular level. Tissue based studies provide information on the differences between structural configuration, ECM organization and the distribution of components throughout the layers while cellular research investigates the role of mechanical stimulation and chemical modulators on the valvular cell activation and signaling pathways through which normal cells switch their phenotypes to the activated diseased and/or calcified cells. The advantage of *in vitro* cell study is the possibility of cell isolation and examination of individual regulators assumed to influence the valve microenvironment; co-culturing VECs and VICs yields an *in vitro* engineered model for the heart valve allowing control of various factors such as substrate material and stiffness, mechanical forces and chemical activators that mimic pathophysiological states of the valve. The following section includes a brief review on tissue and cellular level studies of aortic valve homeostatic and disease mechanisms.

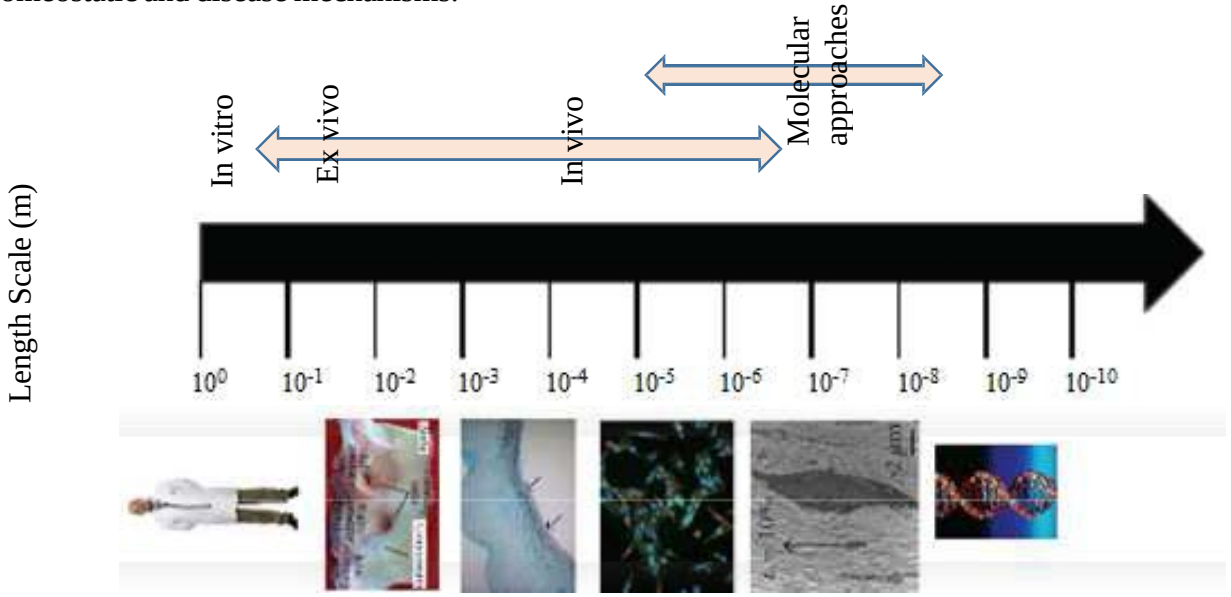

Fig 1.3. Multiscale hierarchy scale recommended for valve mechanobiology and mechanopathology. [23]

1-4 Tissue-Level Studies

Tissue based studies of the valve provide analysis of ECM morphology under different conditions of cyclic stretch, pressure and shear stress. ECM structural alterations (synthesis or degradation) occur as a biological response to its mechanically changing environment that may represent normal or pathological conditions in the valve. In an *ex vivo* study by Balachandran *et al*, valve tissue leaflets were considered in static and stretched exposed conditions [24]. They reported that cyclic stretch increased collagen, decreased sulfated glycosaminoglycans (sGAG), and did not affect elastin contents of the valve ECM. They also indicated that the tri-layer structure of the valve was not altered under stretch. Intriguingly, α-SMA content increased at the ventricular sides of the stretched leaflets, suggesting a possible region with a focal response to mechanical forces. In another study they investigated the role of elevated cyclic stretch on inducing valve disease and showed cell proliferation and apoptosis was directly affected by the cyclic stretch [25]. Their results for matrix remodeling enzymes demonstrated an increase of collagenase, gelatinase, cathepsin S & K and matrix metalloproteinases (MMP) under higher pathological stretch rates (20%) suggesting that increased cyclic stretch may disrupt the homeostatic environment of the valve and contribute to the progression of the disease. They also found that cyclic stretch increased the responsiveness of the serotonin pathway resulting in significant enhancement of matrix remodeling and collagen proliferation.

Thayer *et al* indicated that the combined effect of mechanical stretch and pressure may modulate expression of valve interstitial cell contractile phenotype markers and found that the contractile phenotype was downregulated under hypertensive conditions suggesting that mechanical forces induced during hypertensive condition may stimulate protective mechanisms in the aortic valve tissue [26]

Finally, via alteration of the shear stress environment of the valve, Sucosky *et al* observed upregulation of the expression of inflammatory markers on the aortic side of the leaflets. Their results also suggested that noggin, a BMP-4 inhibitor, was able to mediate these inflammatory responses [27].

1-5 Cell-Level Studies

In studies at the cellular level, cells are isolated from their ECM and cultured on two or three-dimensional substrates. These constructs are stimulated *in vitro* with factors such as mechanical forces and chemical stimulations to mimic the native or pathological environment of the aortic valve disease, followed by analysis of various pathological mechanisms including inflammation, apoptosis, proliferation and osteogenesis. Under these stimulations valvular cells also may switch their phenotypes and express markers specific of the normal or abnormal phases of the injured and remodeled valve.

1-6 Chemical Stimulation Studies at Cell Level

Chen *et al* demonstrated the role of β-catenin on the interaction between wnt and tissue growth factor (TGF-β) signaling pathways in inducing α-SMA transcription and myofibroblast differentiation [28]. They reported that increasing β-catenin through Wnt conditioned medium caused TGF-β to induce higher α-SMA levels (indicative of activated VICs). They also showed that when VICs were cultured on collagen-coated PA gels with physiological stiffness, myofibroblast activation was limited to matrices with fibrosa-like stiffness possibly explaining why the fibrosa is more prone to the disease.

Osman *et al* showed that VICs are capable of differentiating into osteoblast like phenotypes via applying defined mediators such as bone morphogenic proteins (BMP-4, BMP-2) and TGF-β.

Atorvastatin could decrease alkaline phosphatase (ALP) activity and osteoblast differentiation highlighting its potential as a possible therapeutic agent against CAVD [29].

In a study by Metzler *et al*, it was shown that imposing stretch on the VECs caused an upregulation in the expression of proinflammatory markers Intercellular Adhesion Molecule (1ICAM-1) and Vascular Adhesion Molecule 1 (VCAM-1) that are known to be present in the endothelium of the diseased aortic valve [30].

The contribution of TGF-β to aortic valve calcification was studied by Clark *et al* through alizarin red staining, ALP activity and analysis of cell apoptosis. The results showed that VICs treated with TGF-β had significantly more regions stained positive for alizarin red as an indicator of the stenotic diseased VICs. An increased level of ALP activity and higher apoptotic rate induced by TGF-β confirmed the mechanistic role of this osteogentic marker in initiation and progression of the calcific AV [31].

Yip *et al* cultured VICs on gels with different stiffness and found that calcification was regulated by ECM stiffness. They observed that either osteogenic or myofibrogenic differentiation of VICs can result in calcification *in vitro* through two distinct processes respectively mimicking aspects of either bone formation or apoptosis-associated calcification *in vivo* [32].

Signaling pathways such as MPEK/ERK/Rho have also a regulatory effect in aortic valve calcification and their inhibition may reverse the activated or osteogenic VICs to a normal quiescent phenotype [33, 34].

1-7 Mechanical Stimulation Studies at Cell Level

Kloxin *et al* studied the influence of microenvironment activity on myofibroblast activation by culturing VICs on a high modulus activating hydrogel. The authors reported that decreasing the substrate modulus with irradiation reverses this activation, demonstrating that myofibroblasts can be de-activated solely by changing the modulus of the underlying substrate [35].

Balachandran *et al* indicated that EMT (Endothelial Mesenchymal Transformation) of the VECs was elevated under cyclic stretch via increased α-SMA expression and reduced cadherin-positive cells. They also showed that EMT induced tissue generated higher contraction in response to vasoconstrictive drugs indicating the possible regulatory effect of EMT on valve function [36].

The above review contained a brief summary on the role of mechanical and chemical stimulation on mediating valve microenvironment mimicking patho-physiological conditions. However the effect of the cell shape as a physical cue that may intrinsically regulate valve function has not been studied yet. There are several studies for other types of cells that have considered the role of the cell shape on important cellular functions such as cell death and growth, machrophage lineage and stem cell differentiation that will be discussed in the next section.

1-8 Cell Shape on Other Cell Types

The relationship between cell shape, size and organization with cell function have been extensively studied for different cell types. The effect of capillary endothelial cell shape on cell death and growth was studied by Chen *et al* and the results showed that cells cultured on single large circles (20 μm) had a significantly greater apoptosis index than multiple smaller circles while indicating higher growth index values [37]. They also found that integrin ligands regulated the apoptosis rate for unpatterned and patterned cells. Nelson *et al* microfabricated pulmonary endothelial multicellular sheets of square and annulus shape with varying sizes and reported that

the rate and pattern of the proliferation is dependent on the geometry of the monolayer [38]. They also proposed that patterns of mechanical stress may be derived by the organization of the cells and may define various proliferation patterns (depicted in Fig. 1.5). In a comprehensive study by Versaevel *et al* the mechanistic regulation between cell and nuclear shape was investigated emphasizing the role of actin fibers and cell shape area in nuclear remodeling process [39]. They reported that nuclear shape is regulated with the lateral forces generated by the tension in actomyosin fibers that expands as the cells become more elongated. Their results also showed that when intermediate filaments are disrupted for elongated cells, the volume architecture decreased to keep the balance of the intracellular forces. This volume loss that affected chromatin condensation and cell proliferation causing nuclear stiffening. Cells that had a circular shape, however, were not affected by treating with interfilament inhibition, confirming that the nucleus of circular-shaped cells was not altered by tension in actomyosin filaments.

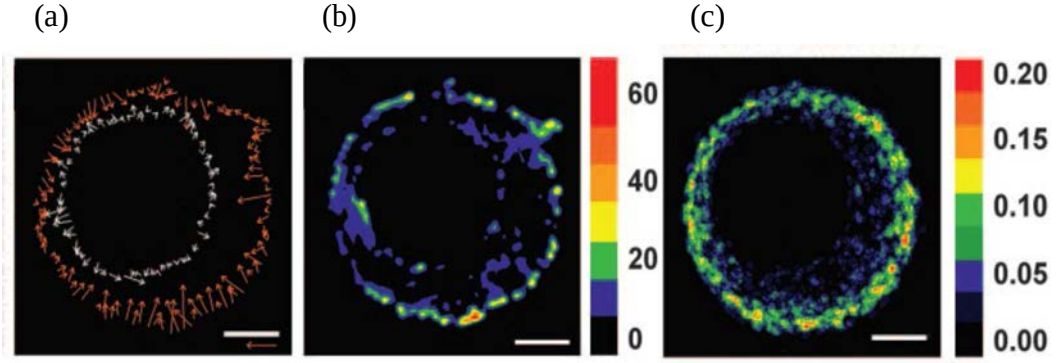

Fig 1.5. Mechanical forces generated by cytoskeletal contraction cause the patterns of proliferation. (a) Vector map of traction forces measured at edges (b) Colorimetric map of traction forces measured over the entire monolayer (nN) (c) Colorimetric images of cell proliferation for cells cultured on asymmetric annulus. [38]

Mcworker *et al* studied the effect of the physical environment on modulation of the proinflammatory (M1) and prohealing (M2) activation states of macrophages [40]. They cultured machrophages on unpatterened (control) and micropatterened surfaces containing different wide lines and found that cell elongation caused the higher expression levels of M2 polarization

markers including arginase-1, CD206 (known as mannose receptor C, type 1), and YM-1 (a machrophage pretein) but did not induce any change in expression of M1- polarization state. They also observed that proinflammatory markers including interleukin (IL). CD54, IFN-γ (interferon), and macrophage inflammatory protein-1α were decreased by cell elongation. They concluded that cell shape itself polarizes macrophages toward an M2 phenotype and that combined with cytokines its effect on polarization state would be enhanced.

Mcbeath *et al* found that commitment of the human mesenchymal stem cells (hMSCs) was mediated by cell shape via RhoA signaling [41]. The cells that were allowed to adhere and spread on the surface differentiated to osteoblasts whereas unspread round cells differentiated into adiopocyets. Active RhoA caused osteogenesis while dominant-negative RhoA induced adiopocyte lineage.

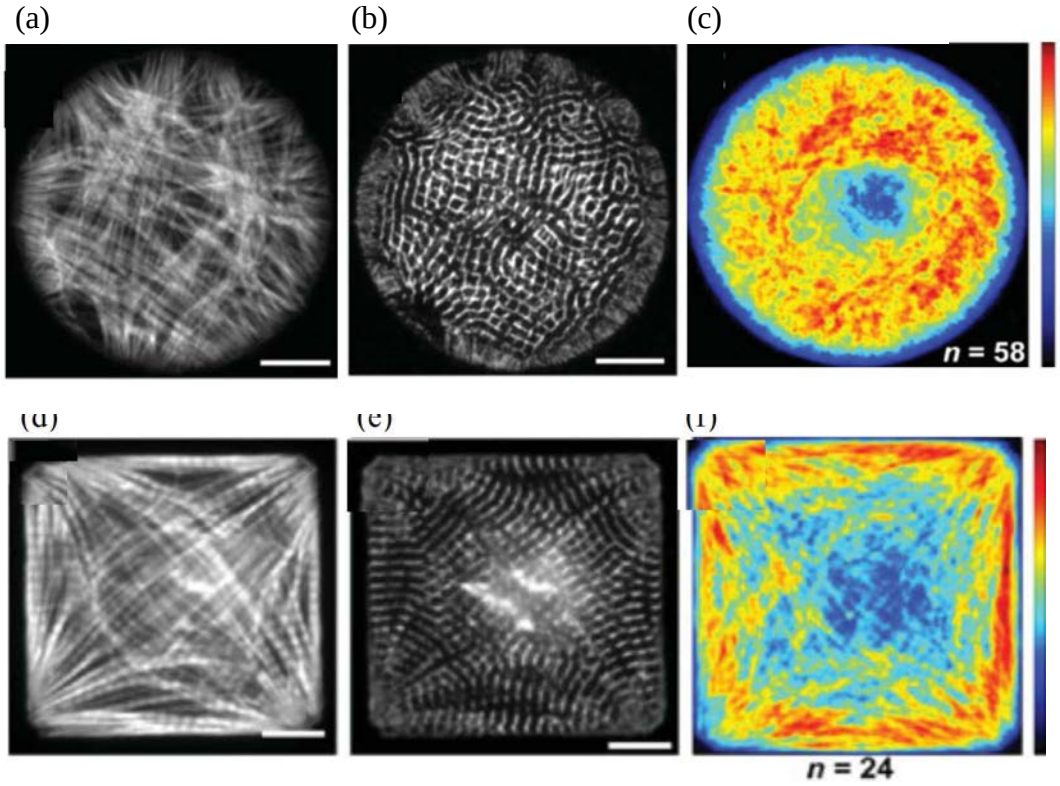

Fig 1.6. The absence of a preferential axis of organization is observed for circular myocytes. (a,d) immunofluorescent stains for F-actin (b,e) immunofluorescent stains sarcomeric a-actinin, (c,f) the averaged distribution of F-actin

Kilian *et al* also investigated the relation between the shape of the hMSCs and cell differentiation [42]. They cultured cells in rectangles with different aspect ratios and pentagonal shapes with various curvatures, and observed that the patterns that promote contractility shifted toward osteoblast while less contraction-inducing patterns differentiated into adiopocytes. Their results also revealed that cytoskeletal disrupting agents modulated the shape dependent commitment of the cells emphasizing the essential role of myosin contractility created in differentiation.

Parker *et al* studied directed cell motility in a cell shape controlled manner [43]. When cells were cultured on the square islands with motility factors, they extended their lamellipodia from the corners with the stress fibers oriented such that the tractional forces focused on the corner regions, indicating the ability of square cells to localize focal adhesions. Bray *et al* considered the effect of cell shape on sarcomere alignment [44]. Myocytes cultured on circular ECM did not align their sarcomeres and actin in predictable patterns while rectangular myocytes assemble predictable and repeatable actin network and aligned sarcomeres. Also, they reported that increasing aspect ratio for rectangular patterns, spatial anisotropy, including aligned myofibrils and the registration of adjacent sarcomeres registration, emerges, introducing myocyte shape as an important potential regulator of myocyte contractility. Alford *et al* cultured vascular small muscle cells (VSMCs) on different rectangular patterns and revealed that cell contractile stress decreased by increasing the pattern width [45]. However the opposite trend was observed for contractile phenotype expression suggesting that phenotype measurement may not be reliably applicable for VSMC contractile behavior.

1-9 Motivation for Thesis

The effect of VIC shape on cellular function and phenotype has not been studied yet. In this thesis, we considered the possible regulatory role of the VIC shape on valve contractile output and phenotype by performing various assays to quantify cell structure, phenotype and contractility.

1-10 Hypothesis and Objectives

We hypothesized that VIC shape can modulate the phenotype and function of the cell.

For proof-of-concept of the hypothesis of this thesis, we stained nuclei of the paraffin embedded sections of normal and calcified human heart valve tissues (obtained from University of Arkansas for Medical Sciences tissue bank) and measured nuclear aspect ratio of the cells. As observed in Fig 3.1, there was a significant difference between healthy and diseased group suggesting the possibility of structural alterations in cell geometry of the valve. Specifically, we noted a decrease in the eccentricity in disease tissue suggesting that there is a reduction in parameters of cellular architecture correlating with disease.

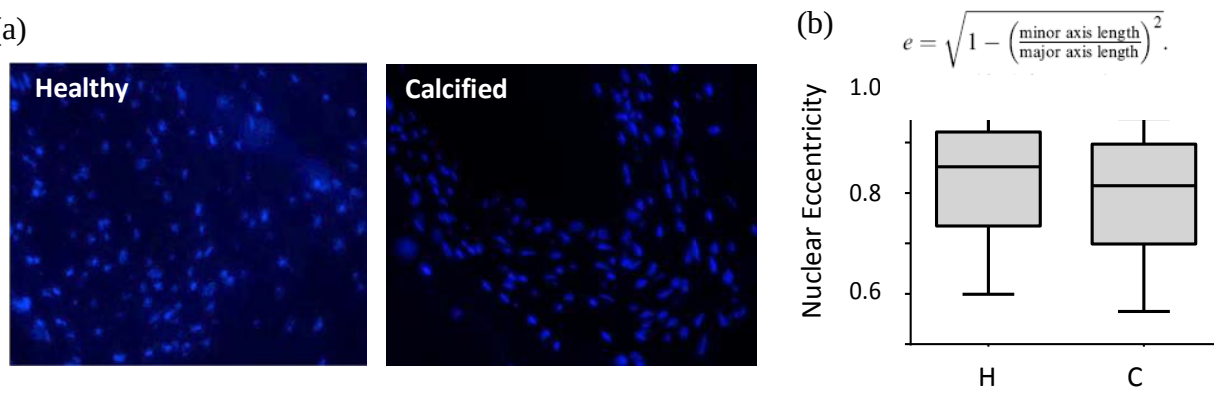

Fig 3.1 (a) Dapi staining of the nuclei for healthy and calcified human aortic valve tissue (b) nuclear eccentricity measurements for healthy and calcified valves (n=3, $p<0.005$)

The hypothesis was examined via four main objectives as listed as below:

1) Design a method to change the shape of the VIC *in vitro*.
2) Quantify change in the cell shape.
3) Analyze change in cell function due to change in shape.
4) Analyze change in cell phenotype due to change in shape.

The experiments performed regarding the objectives are categorized as follows:

1) Mask design, wafer preparation and microcontact printing
2) Immunofluorescent staining of cellular architecture and quantifying metrics for cell shape
3) Valve thin film assay
4) Western blotting and protein expression

Each of these assays will be explained in detail in the following chapter.

CHAPTER TWO

MATERIALS AND METHODS

2-1 Cell Isolation

Fresh porcine aortic valves were obtained from local slaughterhouses (Braunschweig, Neosho, MO and Cockrum, Rudy, AR) and transferred to sterile Phosphate Buffered Saline (PBS, Gibco) on a bucket of ice. Aseptic procedures were adopted upon arrival to the laboratory. The leaflets were dissected and placed in collagenase (Worthington, Lakewood, NJ) and dispase supplemented Hank's Balanced Salt Solution (HBSS) (Gibco, Grand Island, NY) with respective concentrations of 60U/ml and 2U/ml. The solution then was incubated for 2 hours with gentle agitation every 15 mins to extract the valve endothelial cells (VECs). Leaflets were then transferred to fresh enzyme solution, The VEC digestate was not utilized for the experiments in the current project. Fresh enzyme solution was then incubated for two hours as before. Digested VICs were then centrifuged and the cell pellet was suspended in complete media comprising Dulbecco's Modified Eagle Medium (DMEM), 10% fetal bovine serum (FBS), and 1% penicillin/streptomycin and 1% HEPES (all from Gibco) and cultured using standard cell culture methods. All experiments outlined below were performed using cells from passages 3–7.

2-2 Mask Design and Soft Lithography

A photomask was designed using AutoCAD comprising five squares (1.7cm^2). The squares accommodated lines with 10, 20, 40, 60, and 80 μm widths, respectively, spaced by 40 μm gaps. (Fig 2.1) A transparency photomask was manufactured by (Outputcity Inc.) and used to prepare the silicon substrate master via standard photolithography techniques. Briefly, a 10 μm thick layer of SU-8 3005 (Microchem, Westborough, MA) was spin-coated onto a silicon wafer. The

mask was then placed in alignment with the wafer inside the mask aligner (SUS Microtech) and clamps and vacuum were applied to ensure tight contact.

(a) (b)

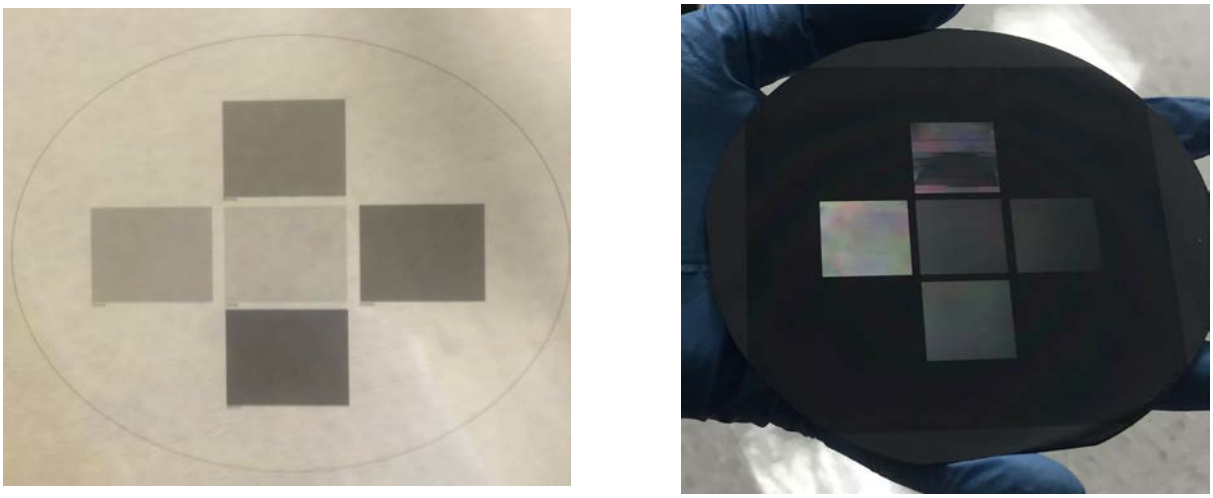

Fig 2.1(a) Mask includes 5 different line widths, designed by AutoCad (b) Silicon wafer with high raised features

Ultraviolet light (wavelength and power) exposure was used to transfer the mask pattern to the wafer. The portion of the uncured SU-8 not exposed to UV light was washed away using SU-8 developer and iso-propyl alcohol. The wafer was then silanized overnight using (Trichlosaline, UCT SPECIALITIES, LLC, Bristol, PA) and the wafer with 10 µm raised rectangular features was ready to use for stamp preparation and soft lithography. (Fig 2.1)

The silicon wafer with rectangular features was first cleaned using acetone, methanol and isopropyl alcohol and dried. 100g of PDMS, polydimethylsiloxane (Sylgard 184 Dow Corning, Midland, MI) was poured over the wafer placed in a petri dish and cured inside oven for at least 4 hours at 65°C. The PDMS template was then removed from the silicon wafer and the individual stamp patterns (i.e. different line widths) were cut out and stored. (Fig 2.2)

(a)

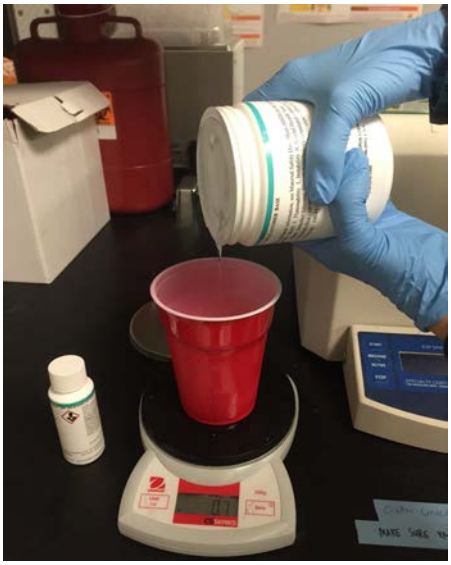

(b)

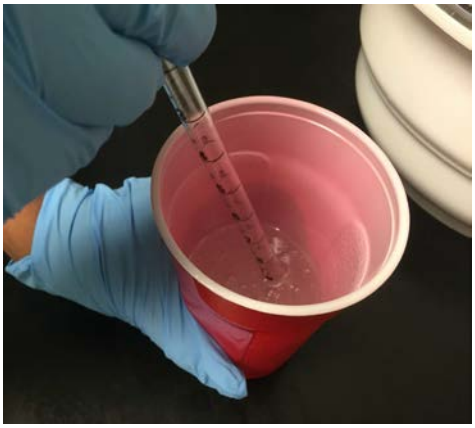

(c)

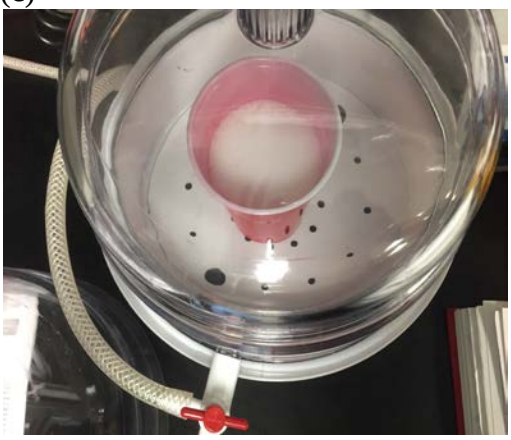

(d)

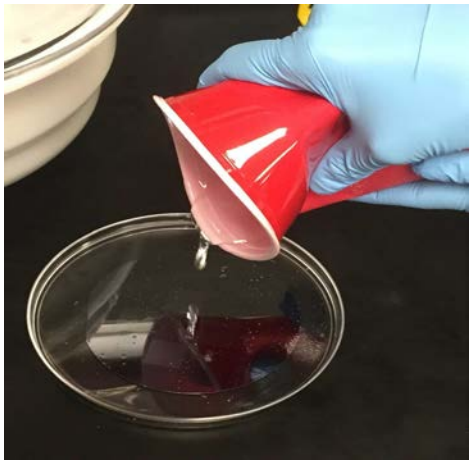

(e)

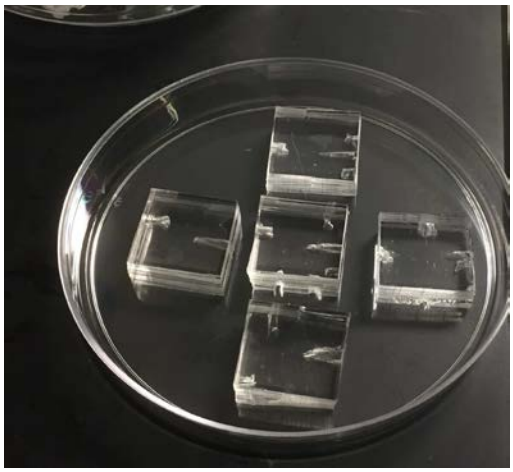

Fig 2.2 Stamp preparation (a) making PDMS solution (b) mixing PDMS and curing agent (c) degassing PDMS through vacuum (d) pouring PDMS on top of the wafer (e) PDMS stamps peeled off of the wafer and cut out

2-3 Micro-contact Printing

2-3-1 Cell Substrate Preparation for Protein Blotting

VICs were seeded on a specially prepared substrate that had the microcontact printed line widths as follows. Substrate was prepared by spin-coating a thin layer of PDMS on a clean 25mm glass coverslip (VWR) and curing overnight at 65°C. PDMS stamps were incubated with 1% Fibronectin solution (Corning) for one hour and then air-dried. PDMS coated substrate was UV-ozone treated for 20 min and the stamps were placed on the substrate surface and pressed slightly to transfer fibronectin features. The stamps then were gently peeled off of the substrate; coverslip substrates then were incubated with 10% pluronic solution for 8-12 min to prevent cell adhesion to the non-fibronectin coated area (gaps between the different line widths) and the VICs were seeded at 500,000-700,000 cells per coverslip.

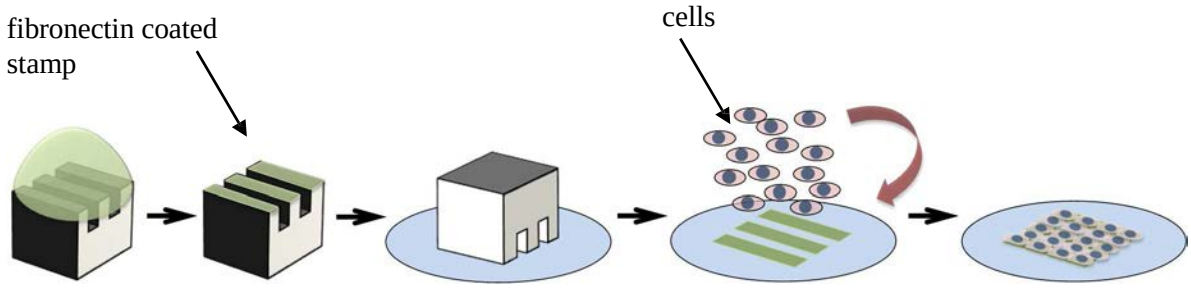

Fig 2.3 Schematic of micro-contact printing technique

The process of wafer fabrication, stamp preparation and micro-contact printing has been summarized in a schematic of Fig 2.4.

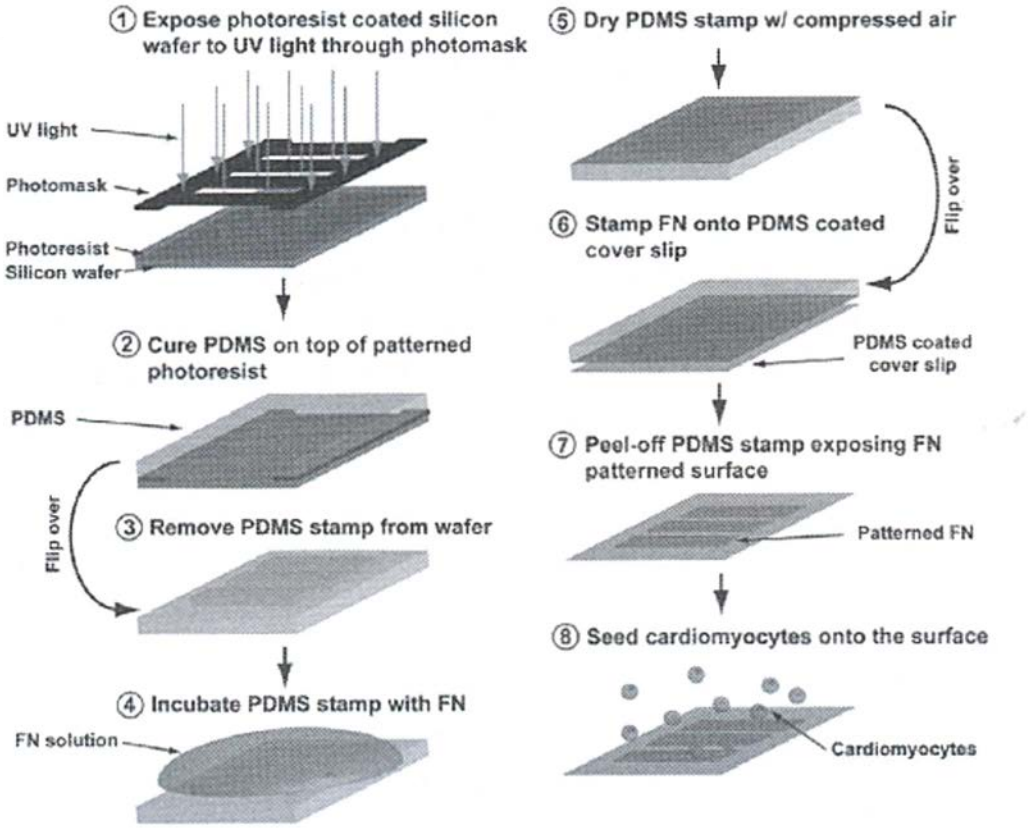

Fig 2.4 Schematic of the stamp fabrication and micro-contact printing process for ECM proteins to PDMS coated coverslips [46]

2-3-2 Cell Substrate Preparation for Valve Thin Film Assay

Substrates were prepared differently for the valve thin film assay as we wished to obtain a freely floating PDMS film that is not attached to the underlying glass coverslip. As the schematic in Fig 2.5 shows, coverglass surface was covered using plastic tape (Patco) and a rectangle was cut off at the center of the coverglass. This rectangular area was spincoated with a thin layer of PIPAAm (Poly-N-Isopropylacrylamide, Sigma-Aldrich, St. Louis, MO/ Polyscience Inc, Warrington, PA);

the remaining tape was peeled away and the coverslip was spin-coated with PDMS as previously described. In this method, no pluronic was needed after printing.

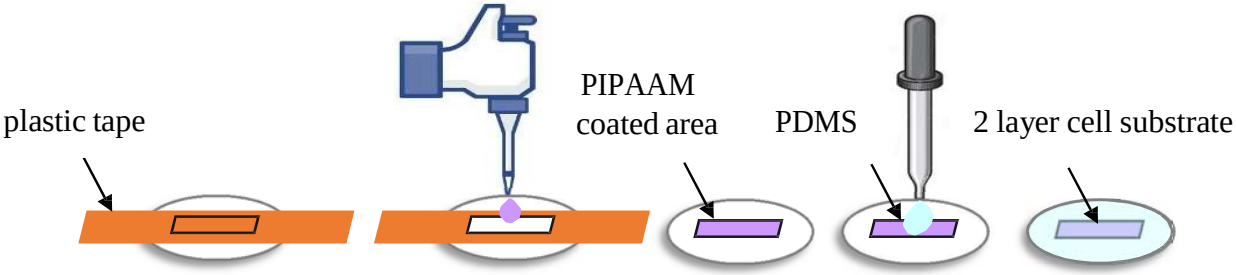

Fig 2.5 Schematic of the substrate preparation for the valvular thin film experiment.

2-4 Valve Thin Film Assay

The valve thin film (vTF) assay follows the protocol utilized for vascular smooth muscle cells [36, 45]. This assay was performed 48 hours after the cell culture in which tissue constructs cultured on coverglass were transferred to a petri-dish containing Tyrode's buffer; the rectangle PIPAAm coated area was cut into strips (films) parallel to the alignment of seeded VICs. The solution was allowed to cool below 32°C to dissolve the PIPAAm layer and release the cell and PDMS layers. Solution temperature was set at 37°C for the duration of the experiment. After 2.5 min of temperature stabiliziation, vTFs were stimulated with 50 nM endothelin-1, a vasoconstrictor, (ET-1, Sigma Aldrich) to curl the films for 15 minutes followed by treatment with 100 μM fasudil, a vasodilator, (HA-1077, Sigma Aldrich) for 30 minutes. The images were taken under a stereoscope (Lecia Microsytems, Buffalo Groves, IL) at 15s intervals and then analyzed using ImageJ (Opensource, NIH) and MATLAB (Mathworks, Natick, MA) to determine radius of curvature and cellular stress required to bend the films (Fig 2.6).

(a) (b)

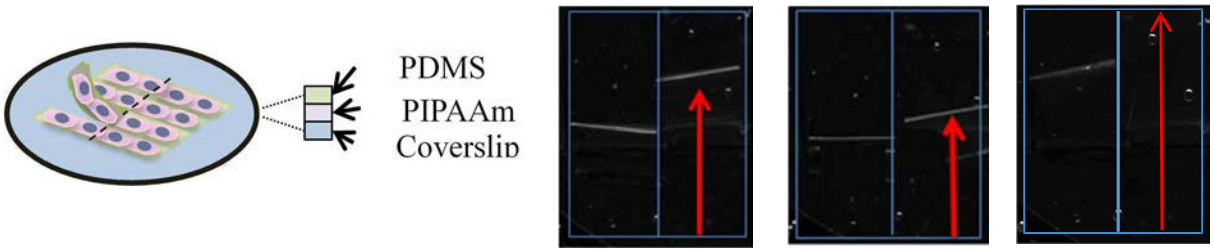

Fig 2.6 (a) Thin films were cut on the PIPAAM layer (b) projection length of the film at the initial state, after ET-1 and HA-1077 treatments.

The length of the film (L) was measured when the film was flattened on the coverslip surface. Eq 2.1(a) was used to numerically measure th e projection length of the film on the coverslip plane (x) and (r) at each time point. Eq 2.1(b) measures the stress (σ) having the following parameters:

(E): PDMS elastic modulus, (t): PDMS thickness, (h): Tissue thickness, (υ): Poisson's ratio of PDMS and (r): Radius of curvature derived from Eq 2.1(a).

(a) (b)

$$x = \begin{cases} r\sin\left(\frac{L}{r}\right) \in \frac{2L}{\pi} < x < L \\ r \in \frac{L}{2\pi} < x < \frac{2L}{\pi} \end{cases} \qquad \sigma = \frac{Et^3}{6R(1-\nu)h^2(1+t/h)} \qquad \text{Eq 2.1}$$

2-5 Fluorescent staining for cell and nuclear architecture analysis

Cells were fixed and stained for nuclei (DAPI, Life Technologies) and F-actin (phalloidin, Life Technologies) and imaged using a regular upright inverted microscope at 40X magnification for analysis of actin alignment. Actin alignments were quantified by analyzing the phalloidin stained images in MATLAB. The program, updated by Dr. Balachandran, was a customized version of a fingerprint detection algorithm (Peter Kovesi, University of Western Australia) in which actin filaments were detected as ridge-like regions and the ridge-mask coupled with vectors oriented along the ridges was used to give the orientation parameter as a quantitative measurements for

the alignment. Orientation parameter ranges from 0 for un-aligned isotropic filaments to 1 for perfectly aligned filaments.

Nuclear eccentricity was analyzed using a custom-developed MATLAB code [36]. Eccentricity is a normalized measure for the aspect ratio of the nucleus, where 1 represents a 1-dimensional line and 0 represents a perfect circle. The equation for eccentricity is shown as Eq. 2.2.

$$\varepsilon = \sqrt{1 - \left(\frac{\text{minor axis length}}{\text{major axis length}}\right)^2}. \qquad \text{Eq 2.2}$$

Cells from separate experiments were live-stained with GFP-plasma membrane stain (Life Technologies) and similarly imaged. Cell aspect ratio was quantified via images of the live stained plasma membrane in ImageJ by manually fitting an ellipse to the cell membrane and measuring major and minor axes values.

Actin, nuclear and cell aspect ratio parameters were quantified for at least ten images per sample from a total of 4-6 samples.

2-6 Western Blotting

Western blotting allows quantitative measurement of the proteins of interest using specific antibodies. Prior to western blot, cell lysate containing the proteins were collected using RIPA buffer (Santa-Cruz, Santa Cruz, CA) and centrifuged at 21,000 rpm to pellet the cell debris. The supernatant was analyzed via BCA protein assay to quantify the protein concentration. Following protein assay, equal amounts of the proteins (35 µg) were separated based on their molecular weights using Sodium Dodecyl Sulfate Polyacrylamide Gel Electrophoresis (SDS-PAGE) in a 4-15% gel at 200V constant voltage. Proteins were then transferred to a Polyvinyl Fluoride (PVDF) membrane at 150V constant voltage at 4°C. The membranes were incubated in blocking

buffer (LI-COR Biosceince, Linclon, NB), primary and IR-Dye conjugated secondary antibody solutions and scanned using a LiCor Odyssey scanner (LI-COR). The obtained images of the membranes then were analyzed through ImageJ to quantify protein expression by measuring the intensity of the expressed protein bands. The antibodies used, and their respective concentrations are tabulated in Table 2.1.

Antibody	**Concentration**
α-SMA	1:100
Vimentin	1:100
Smooth Muscle Heavy Chain (SMMHC)	1:25
β-actin	1:1000

Table 2.1 Antibodies used for western blot and their relative concentrations

2-7 Statistical Analysis

All data was presented as mean ± standard error. Minitab software (Minitab release 14, Minitab Inc. State College, PA), Excel (Microsoft Corp, Bellevue, WA) and Prism (GraphPad Software Inc, La Jolla, CA) were used for the analyses. The difference between the samples were assumed significant if the p-value < 0.05. Student t-tests were used for testing the difference between sample groups when the data follow a normal distribution, and only two groups are being compared. ANOVA was applied for the analysis with Tukey's post-hoc test for the comparison between more than two groups. For data not normally distributed, Kruskal-Wallis and Dunn's method on pairwise comparisons were used replacing student t-tests and ANOVA respectively.

CHAPTER THREE

RESULTS

3-1 *In vitro* model for altered cell shape

As we mentioned earlier, to prepare an *in vitro* model of the various cell shapes, we designed a mask from which a silicon wafer was fabricated and utilized as a template for making PDMS stamps. The stamps were used in micro-contact printing and formed the desired high raised lines on the cell substrate. Fig 3.1 shows the pictures of the cells aligned into five different line widths.

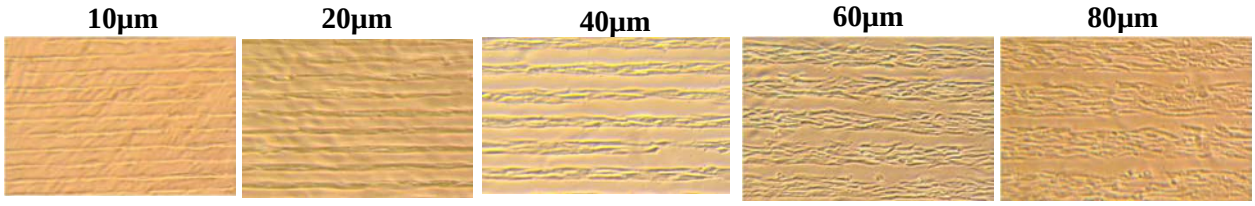

Fig 3.1 Bright field images of VICs micro-patterned into thin tissue lines of different widths, separated by 40 mm gaps.

3-2 Role of cell shape on valve interstitial cell architecture

We designed structural patterns for the VICs including rectangles of 5 different widths and asked if these patterns could indicate similar variations in cellular geometry and organization. Structural analysis was performed for the actin alignment and cell shape by staining actin filaments and nuclei and measuring orientation parameter (OP) and cell aspect ratio. As depicted in Fig. 3.2, a trend for decreasing OP and cell aspect ratio was seen by increasing the pattern width. Results showed that actin architecture was more than 80% aligned (OP>0.8) for all the patterns. However there was a significant difference between narrow patterns (10 and 20) and wide patterns (40, 60, and 80).

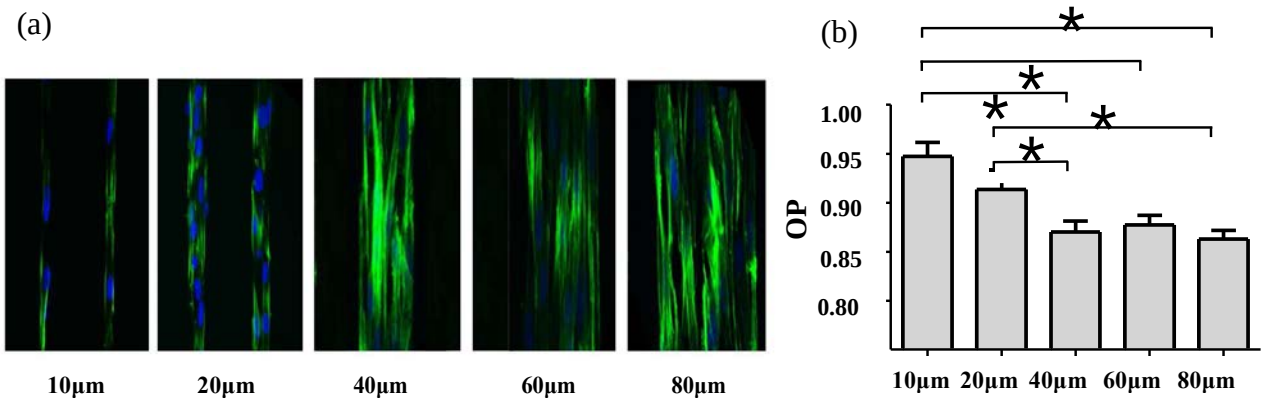

Fig 3.2 Histochemical analysis of different tissue constructs. (a) Actin filaments stained for phaloidin and nuclei stained for DAPI (b) Alignment of the actin filaments was measured by Orientation Parameter (OP)

Cell aspect ratio was obtained by live staining of the cell membrane. Using ImageJ, each cell was estimated with an ellipse and the aspect ratio was determined by dividing minor axis to the major axis of the ellipse. Results showed dominant variations changing from high values of 10 for 10µm width to 4 for 80µm width. Statistical analysis revealed significant difference between almost all of the groups. (Fig 3.3) Nuclear eccentricity data obtained from DAPI staining of the tissue patterns and similar to the aspect ratio values, had significant difference between almost all of the groups. Nuclear eccentricity was higher for thinner patterns and were reduced by increasing the pattern width (Fig 3.3).

We also noted that there was a correlation between cell aspect ratio and nuclear eccentricity that was in agreement with other studies. [45, 47]

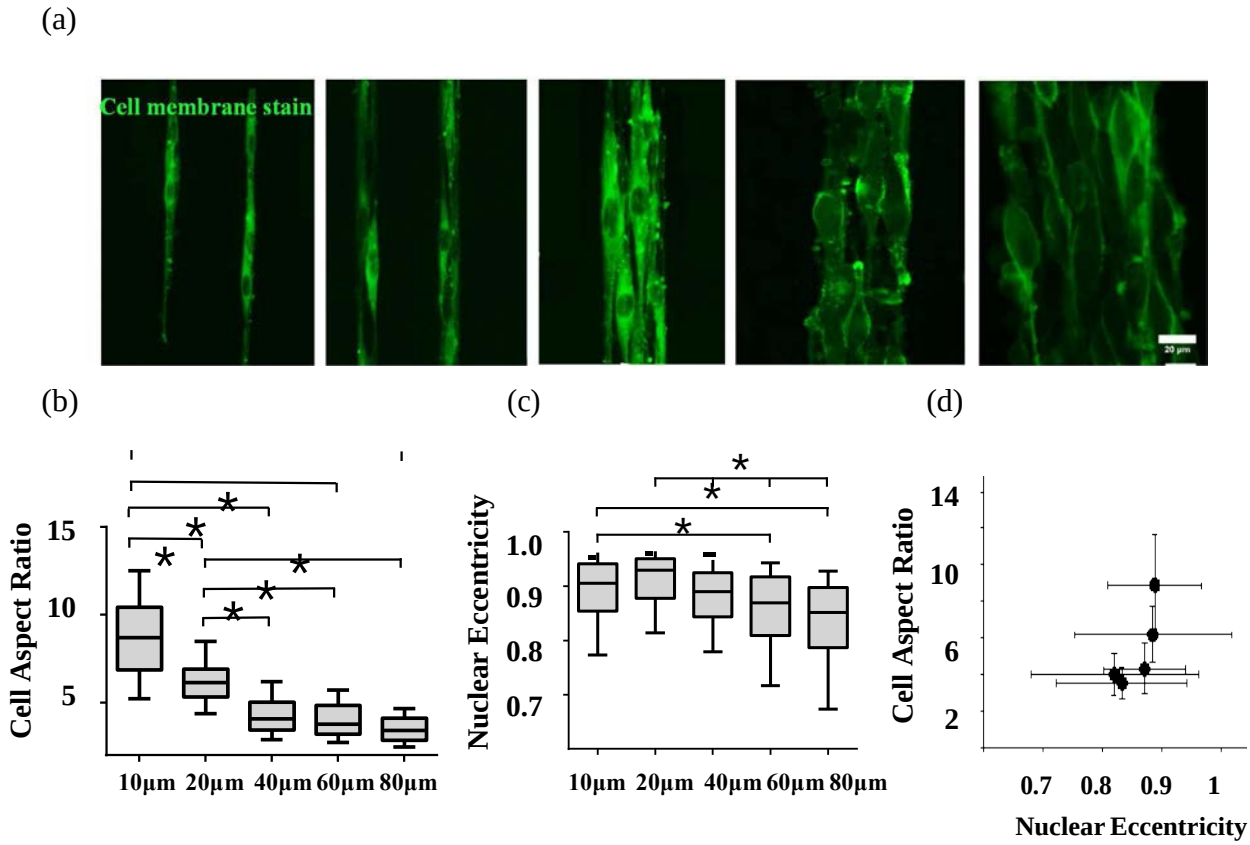

Fig 3.3 (a) Membrane of the cells live stained and imaged with green plasma membrane stain (b) cell aspect ratio(c) nuclear eccentricity(d) Correlation between cell aspect ratio and nuclear eccentricity (r=0.9, p=0.08) (*: statistical difference<0.05)

3-3 Role of cell shape on valve interstitial cell function

As the next step, functional behavior of the VICs were studied via the valvular thin film assay (vTF) and stress values were calculated for all the patterns. As illustrated in Fig 3.3, all the tissue patterns responded to the stimulation. ET-1 induced contraction and increased the stress and HA-1077 caused the films to relax and reduced the stress. Maximum contraction and basal tone were calculated and demonstrated in Fig 3.4. One way ANOVA of contraction stress compared stress values for various pattern widths and confirmed that they were not significantly different. However comparison of basal tone between them revealed statistical differences between 10µm and 40µm and also 40µm and 60µm. (Fig 3.9)

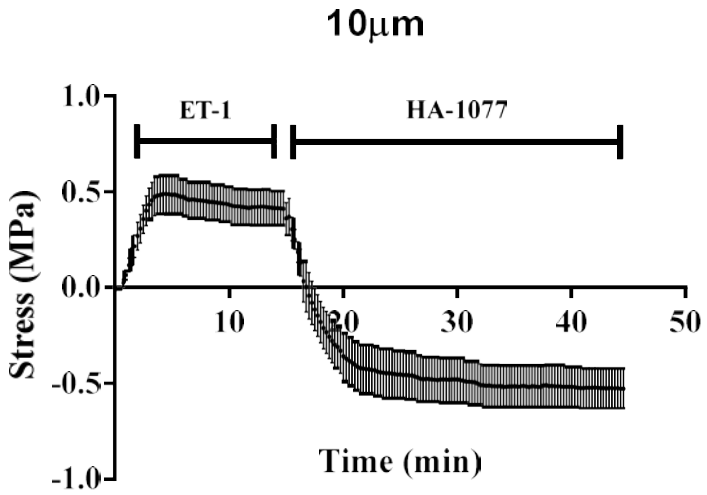

Fig 3.4 Temporal apparent stress for serial stimulations of 10μm VTFs with endothelin 1 followed by HA-1077

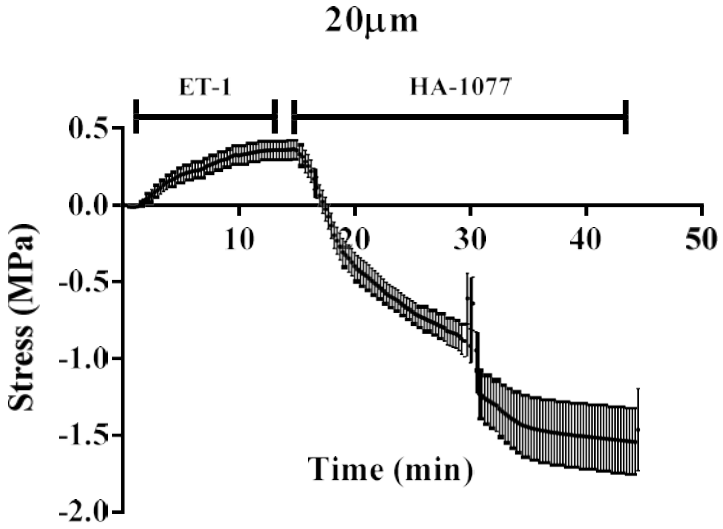

Fig 3.5 Temporal apparent stress for serial stimulations of 20μm VTFs with endothelin 1 followed by HA-1077

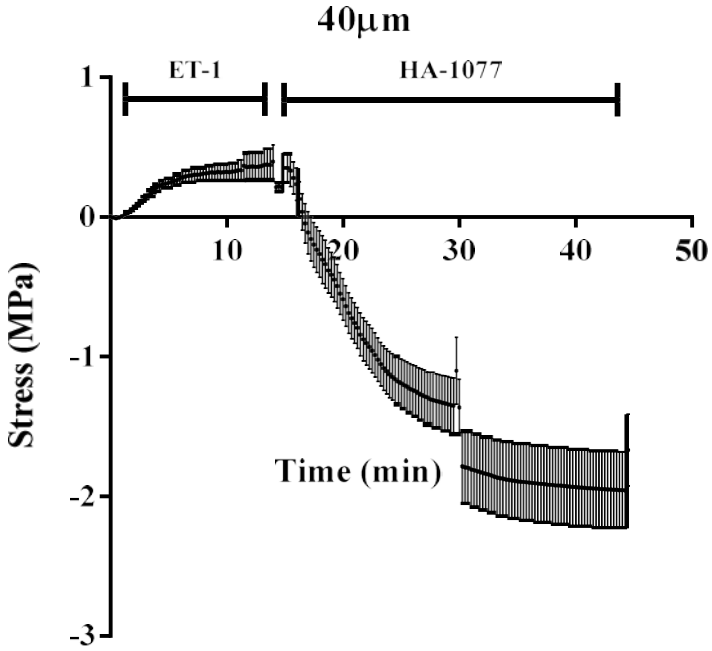

Fig 3.6 Temporal apparent stress for serial stimulations VTFs with 40µm of endothelin 1 followed by HA-1077

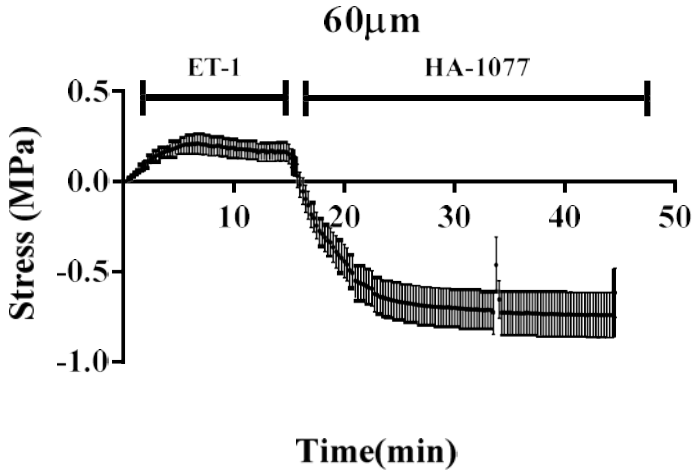

Fig 3.7 Temporal apparent stress for serial stimulations of 60µm VTFs with endothelin 1 followed by HA-1077

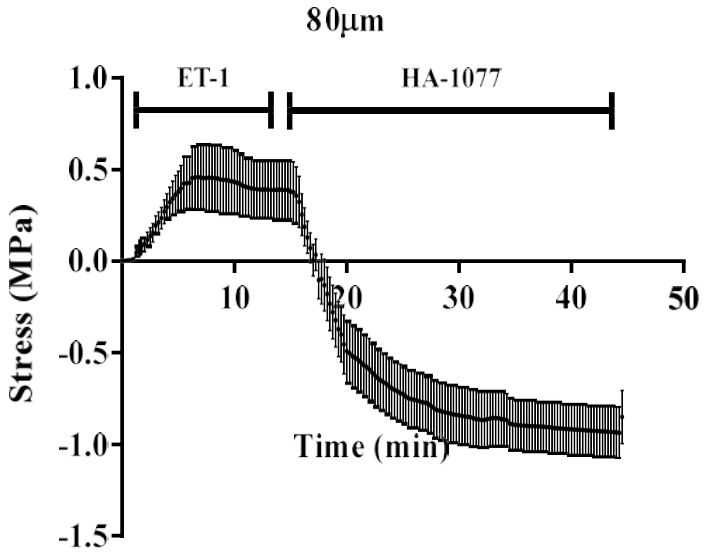

Fig 3.8 Temporal apparent stress for serial stimulation of 80μm VTF with endothelin-1 followed by HA-1077

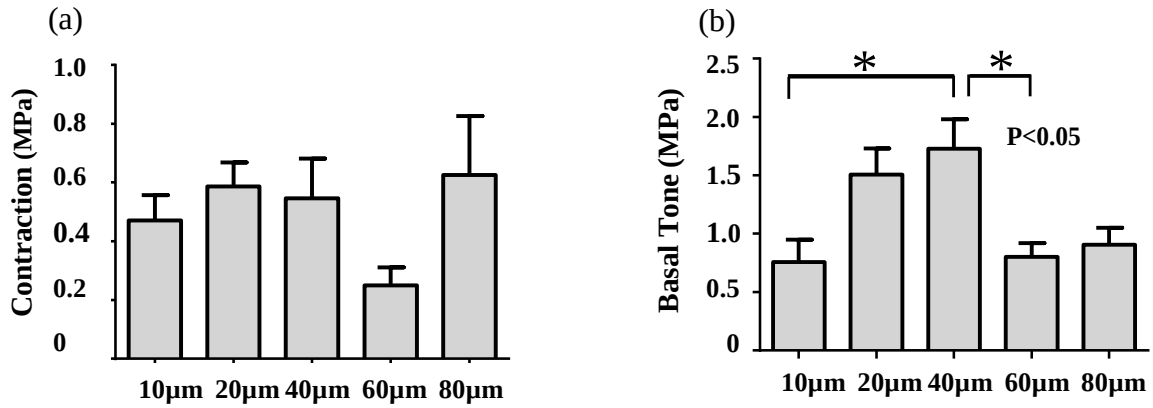

Fig 3.9 (a) Tissue contraction induced by 50 nM ET-1 stimulation for all tissues. (b) Basal contractile tone for all tissues.

3-4 Role of cell shape on valve interstitial cell phenotype

Phenotypic study of the VICs was investigated by western blotting. Western blot allows to analyze the expression of the proteins specific of contractile and activated phenotype. Three proteins were analyzed including α-Smooth Muscle Actin (α-SMA), Vimentin (Vim) and Smooth muscle heavy chain (SM-MHC). These proteins are recognized as the markers of contractile and activated phenotypes. We used to these proteins to determine if the changes in

contractile behavior of the VICs was induced by their phenotypic switching. Table 3.1 shows these antibodies and their relation to myofibroblasts and smooth muscle cells. SMMHC and Vim are recognized as contractile markers and α-SMA as the marker for activated phenotype.

α-SMA and Vim did not follow a decreasing or increasing trend. A trend for increasing SMMHC expression was observed by increasing the pattern width. No statistically significant difference were apparent between different groups for all the phenotypes. These results suggest the phenotype was mixed within our samples and therefore may not be a reliable indicator of the contractile function of the cells.

Antibody	Filament System	Activated Myofibroblasts	Smooth Muscle Cells
Vimentin	**Intermediate / mesenchymal**	**+**	**+/-**
α-SMA	**Microfilament actin**	**+/-**	**+**
SM1 + 2	**Myosin heavy chain**	**-**	**+**

Table 3.1 Antibodies used to describe activated and smooth muscle cell phenotype

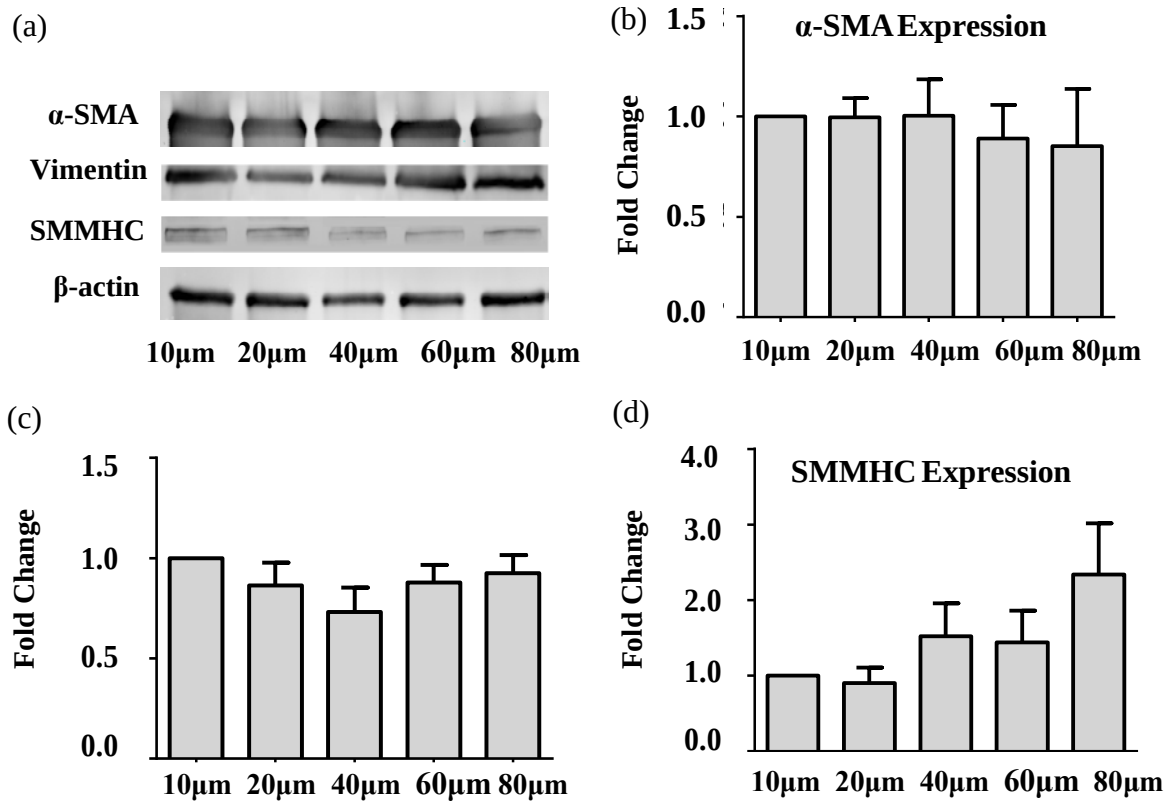

Fig 3.10 Western blot for contractile markers, α-SMA, Vimentin, and smooth muscle myosin heavy chain (SMMHC). Normalized quantified expression with β-actin for (b) α-SMA, (c) Vimentin, and (d) SMMH

CHAPTER FOUR

DISCUSSION

A discussion our results and limitations are presented below. Using micro-contact printed tissue patterns with constrained boundary conditions, we studied the cell shape alteration, cell phenotype, cell functional stress and the possible relationship between them.

Cell aspect ratio varied significantly depending on the pattern width used, however their differences seemed not to have a large effect on contractile behavior and cell phenotype. Cell aspect ratio varied from approximately 10 for thinnest pattern to 5 for the widest. All these patterns depicted a spindle shape in this range. If the VICs were able to adopt a rhomboid or circular shape, more variation may have been observable in the expression of protein markers and functional behavior. This was probably an indication of the stable nature of the VIC shape, function and phenotype. Future studies should therefore consider longer culture durations than 48 hours to examine if there are significant changes in VIC function and phenotype due to altered cell shape.

Orientation parameter indicated high alignment for all the patterns with a trend for decreasing in wider patterns that is due to the higher cell density. When cells were restricted into thin lines (10 and 20) less number of cells were present and actin filaments have less space to spread out forcing them to align in almost the same direction having higher alignment. The significant difference between the alignments of the different tissue lines may explain the role of the cytoskeletal organization on functional differences of the cells.

Phenotypic switching of the heart valve cells is traditionally considered to be indicative of normal or diseased conditions. Quiescent VICs (qVICs) have been characterized as having

synthetic phenotypes. These VICs are observed in a normal adult aortic valve and exhibit little or no cell proliferation and control valve homeostasis through mediating ECM collagen thickness and alignment [4]. Under injury or disease, qVICs become activated and possess characteristics of myofibroblasts exhibiting elevated contraction, stress fibers and contractile proteins such as α-SMA, vimentin and myosin heavy chain that are not present in qVICs [48, 49]. Myofibroblasts have been shown to affect ECM remodeling [49, 50], cell proliferation and migration [51] and are also related to apoptosis [52]. Vimentin is a type III intermediate filament covering the heart chambers and inner surfaces of large blood vessels. Based on Schnittler *et al*, the content of vimentin was predominantly higher in more dynamic environments such as the aorta, pulmonary trunk and left ventricle as compared to lower stress hemodynamic environments such as vena cava, atria and right ventricle, suggesting the adaptive response of the cytoskeleton to the changing mechanical loading by the possible role of the vimentin in helping endothelial cells to endure high blood pressure and flow. [53]

In this research work we investigated the expression of these three markers and their possible role in altering valvular function. Our results showed that smooth muscle myosin heavy chain (SMMHC) and α-SMA were expressed for all the patterns showing their capability in stimulating the diseased phenotype. Vimentin was also strongly expressed for all the tissue constructs confirming the possible existence of the qVICs. However we could not clearly distinguish qVICs, as both aVICs and qVICs express Vimentin [49]. SMMHC is recognized as the basic marker of contractile SMC and was expressed at a lesser extent than Vimentin and α-SMA for all the tissue patterns confirmed by previous studies verifying SMC expression in the aortic valve [54] and the basement of the ventricularis [55, 56]. Again, since α-SMA is shared by both aVIC and SMCs, activated myofibroblasts cannot be differentiated from SMCs. It is therefore

suggested that VICs are isolated separately from different layers of the valve (fibrosa, spongiosa, ventricularies) during cell harvest to allow for differentiating various cell phenotypes (quiescent, activated myofibroblasts and smooth muscle like cells) and to provide a comparison between functional behavior of the layers at the cellular level. This may also render a more accurate phenotype of the cells observable in *ex vivo* conditions. Comparing the expression of the proteins between all the patterns did not reveal a significant difference, suggesting that VICs exist as a continuum of phenotypes *in vitro*. However a trend for increasing SMMHC may suggest that wider patterns may promote pathological conditions leading to aortic valve disease initiation and progression [16].

The results from this thesis also are in agreement with other studies that higher cell-cell contact, in wider patterns here, cause an increase in contractile phenotype [45, 57, 58]. Stress data for the patterns followed an almost similar trend to the phenotype curves however there are some deviations for 60μm lines in the contraction regime and wider lines (60μm and 80μm) in basal tone suggesting that contractility of the tissue may not be induced by phenotype alterations as assumed previously and that there may be some other factors besides the actin and nuclear cytoskeleton in determining the mechanical features and consequently functional behavior of the cells.

Moreover it was noted that both cell elongation and cell-cell contact act to increase the cell contractility. Cells were more elongated and have higher aspect ratio in thinner patterns and more cell-cell contact exist in wider patterns. The results for the contractile basal tone may therefore suggest that both of these effects may have produced the maximum value for 40μm lines as the middle range line width. However further investigation is required to separately consider and quantify cell-cell contact and its relevance to the heterogeneity of the stress

response in contraction and basal tone. Moreover cell coverage percentage is another factor that may affect the accuracy of the results. Lower stress data may arise from the fact that lower surface area of the cells have been covered by the cells. If this area would be measurable during the thin film experiment, stress values could have been normalized by that metric, thereby providing more reliable results to compare the differences between various pattern widths.

Focal adhesions (FA) are macromolecular assemblies that transmit mechanical forces and regulate signals between the ECM and the interacting cell. FA size has been recognized to transduce cell shape signals into contractility by controlling cellular traction and reported to have a significant effect on cell survival [37, 59-61]. Another study showed that the mechanical output of the cell was regulated by spread area alone. They reported that despite having an increased number of focal adhesions as a result of increasing spread area, FA number was associated with an increase in strain-energy for unconfined geometries and concluded that FA may not regulate the mechanical work done by the whole cell [61]. Based on the above mentioned studies it is recommended to consider the effects that focal adhesion size and number may have on cell shape and functional stress for further studies of this work.

CHAPTER FIVE

Conclusions and Future Directions

This study indicated the effect of the geometry of the valve interstitial cells on the functional cell behavior and phenotype. The findings of this work can be outlined as follows:

- We could successfully construct tissue *in vitro* with various structural organizations. Orientation parameter, cell aspect ratio and nuclear eccentricity data varied among different tissue pattern widths.
- Valve thin film functional assay indicated that cells were responsive to chemical stimulations induced by vasoconstriction and vasodilation drugs.
- The contractility behavior of the VICs was likely influenced by the cell elongation and cell-cell contact; the former more dominant in thinner patterns and the latter in wider patterns that may be correlated to the variations of the contraction and basal tone for the patterns.
- Basal tone had the maximum value for 40μm patterns in which the effects of cell-cell contact and cell elongation may have optimally superposed.
- Phenotype did not significantly vary between the patterns suggesting that functional changes were due to the alteration of shape alone.

The following suggestions may be considered as future directions of this work:

- Assessing the cell coverage area for the thin film assay:

  Some empty spaces may be observable on the cell substrate after the cell culture due to improper micro-contact printing and artifacts of the wafer that has transferred to the

stamps. This may affect the amount of the stress generated by the cells and can be included in stress assessment by normalizing the stress with the cell coverage percent.

- Determining cell and PDMS thickness for each thin film experiment:

  In this study we assumed the thickness of the myocardium for the VICs. It is recommended to calculate the thickness of the tissue for each individual patterns using live or fixed and fluorescently stained cells combined with confocal z-stack imaging. Moreover the thickness of the PDMS (t) is changing with the curing time prior to spin-coating [62] for the cell substrate preparation (described in section 2-3) and the stress value (σ) in Eq 2.1 is proportional to t^3 confirming the significance of having an accurate thickness for the stress measurements. Thus it is recommend to directly measure the PDMS thickness using a profilometer.

- Running western blot for the other proteins markers:

  In this study we studied three markers of contractile and smooth muscle cell phenotype. Considering the markers for calcification and inflammation such as OPN, OCN, ICAM, VCAM, and signaling pathways such as ERK and TGF-β may explain if the patterns can mimic calcified conditions of the valve.

- Performing the experiments in longer periods after the culture (5-7-14 days):

  This will allow us to consider how time may influence the changes in cell function and phenotype.

- Investigating the focal adhesion and its role on regulating the cell shape.

REFERENCES

1. Chen, J.H. and C.A. Simmons, *Cell-matrix interactions in the pathobiology of calcific aortic valve disease: critical roles for matricellular, matricrine, and matrix mechanics cues.* Circ Res, 2011. 108(12): p. 1510-24.

2. Combs, M.D. and K.E. Yutzey, *Heart valve development: regulatory networks in development and disease.* Circ Res, 2009. 105(5): p. 408-21.

3. Roger, V.L., et al., *Heart disease and stroke statistics--2011 update: a report from the American Heart Association.* Circulation, 2011. 123(4): p. e18-e209.

4. Aikawa, E., et al., *Human semilunar cardiac valve remodeling by activated cells from fetus to adult: implications for postnatal adaptation, pathology, and tissue engineering.* Circulation, 2006. 113(10): p. 1344-52.

5. Leopold, J.A., *Cellular mechanisms of aortic valve calcification.* Circ Cardiovasc Interv, 2012. 5(4): p. 605-14.

6. Ben-Dor, I., et al., *Correlates and causes of death in patients with severe symptomatic aortic stenosis who are not eligible to participate in a clinical trial of transcatheter aortic valve implantation.* Circulation, 2010. 122(11 Suppl): p. S37-42.

7. Edep, M.E., et al., *Matrix metalloproteinase expression in nonrheumatic aortic stenosis.* Cardiovasc Pathol, 2000. 9(5): p. 281-6.

8. Schoen, F.J., *Evolving concepts of cardiac valve dynamics: the continuum of development, functional structure, pathobiology, and tissue engineering.* Circulation, 2008. 118(18): p. 1864-80.

9. Hinton, R.B., Jr., et al., *Extracellular matrix remodeling and organization in developing and diseased aortic valves.* Circ Res, 2006. 98(11): p. 1431-8.

10. Rabkin, E., et al., *Activated interstitial myofibroblasts express catabolic enzymes and mediate matrix remodeling in myxomatous heart valves.* Circulation, 2001. 104(21): p. 2525-32.

11. Sacks, M.S., W. David Merryman, and D.E. Schmidt, *On the biomechanics of heart valve function.* J Biomech, 2009. 42(12): p. 1804-24.

12. Tompkins, R.G., J.J. Schnitzer, and M.L. Yarmush, *Macromolecular transport within heart valves.* Circ Res, 1989. 64(6): p. 1213-23.

13. Muller, A.M., et al., *Expression of endothelial cell adhesion molecules on heart valves: up-regulation in degeneration as well as acute endocarditis.* J Pathol, 2000. 191(1): p. 54-60.

14. Butcher, J.T. and R.M. Nerem, *Valvular endothelial cells regulate the phenotype of interstitial cells in co-culture: effects of steady shear stress.* Tissue Eng, 2006. 12(4): p. 905-15.

15. Liu, A.C., V.R. Joag, and A.I. Gotlieb, *The emerging role of valve interstitial cell phenotypes in regulating heart valve pathobiology.* Am J Pathol, 2007. 171(5): p. 1407-18.

16. Latif, N., et al., *Expression of smooth muscle cell markers and co-activators in calcified aortic valves.* Eur Heart J, 2015. 36(21): p. 1335-45.

17. Mathieu, P., et al., *Calcification of human valve interstitial cells is dependent on alkaline phosphatase activity.* J Heart Valve Dis, 2005. 14(3): p. 353-7.

18. Steitz, S.A., et al., *Osteopontin inhibits mineral deposition and promotes regression of ectopic calcification.* Am J Pathol, 2002. 161(6): p. 2035-46.

19. Rajamannan, N.M., et al., *Human aortic valve calcification is associated with an osteoblast phenotype.* Circulation, 2003. 107(17): p. 2181-4.

20. Kaden, J.J., et al., *Expression of bone sialoprotein and bone morphogenetic protein-2 in calcific aortic stenosis.* J Heart Valve Dis, 2004. 13(4): p. 560-6.

21. Yao, Y., et al., *Inhibition of bone morphogenetic proteins protects against atherosclerosis and vascular calcification.* Circ Res, 2010. 107(4): p. 485-94.

22. Levy, R.J., et al., *Biologic determinants of dystrophic calcification and osteocalcin deposition in glutaraldehyde-preserved porcine aortic valve leaflets implanted subcutaneously in rats.* Am J Pathol, 1983. 113(2): p. 143-55.

23. Balachandran, K., P. Sucosky, and A.P. Yoganathan, *Hemodynamics and mechanobiology of aortic valve inflammation and calcification.* Int J Inflam, 2011. 2011: p. 263870.

24. Balachandran, K., et al., *An Ex Vivo Study of the Biological Properties of Porcine Aortic Valves in Response to Circumferential Cyclic Stretch.* Ann Biomed Eng, 2006. 34(11): p. 1655-65.

25. Balachandran, K., et al., *Elevated cyclic stretch induces aortic valve calcification in a bone morphogenic protein-dependent manner.* Am J Pathol, 2010. 177(1): p. 49-57.

26. Thayer, P., et al., *The effects of combined cyclic stretch and pressure on the aortic valve interstitial cell phenotype.* Ann Biomed Eng, 2011. 39(6): p. 1654-67.

27. Sucosky, P., et al., *Altered shear stress stimulates upregulation of endothelial VCAM-1 and ICAM-1 in a BMP-4- and TGF-beta1-dependent pathway.* Arterioscler Thromb Vasc Biol, 2009. 29(2): p. 254-60.

28. Chen, J.H., et al., *beta-catenin mediates mechanically regulated, transforming growth factor-beta1-induced myofibroblast differentiation of aortic valve interstitial cells.* Arterioscler Thromb Vasc Biol, 2011. 31(3): p. 590-7.

29. Osman, L., et al., *Role of human valve interstitial cells in valve calcification and their response to atorvastatin.* Circulation, 2006. 114(1 Suppl): p. I547-52.

30. Metzler, S.A., et al., *Cyclic strain regulates pro-inflammatory protein expression in porcine aortic valve endothelial cells.* J Heart Valve Dis, 2008. 17(5): p. 571-7; discussion 578.

31. Clark-Greuel, J.N., et al., *Transforming growth factor-beta1 mechanisms in aortic valve calcification: increased alkaline phosphatase and related events.* Ann Thorac Surg, 2007. 83(3): p. 946-53.

32. Yip, C.Y., et al., *Calcification by valve interstitial cells is regulated by the stiffness of the extracellular matrix.* Arterioscler Thromb Vasc Biol, 2009. 29(6): p. 936-42.

33. Gu, X. and K.S. Masters, *Role of the MAPK/ERK pathway in valvular interstitial cell calcification.* Am J Physiol Heart Circ Physiol, 2009. 296(6): p. H1748-57.

34. Gu, X. and K.S. Masters, *Role of the Rho pathway in regulating valvular interstitial cell phenotype and nodule formation.* Am J Physiol Heart Circ Physiol, 2011. 300(2): p. H448-58.

35. Kloxin, A.M., J.A. Benton, and K.S. Anseth, *In situ elasticity modulation with dynamic substrates to direct cell phenotype.* Biomaterials, 2010. 31(1): p. 1-8.

36. Balachandran, K., et al., *Cyclic strain induces dual-mode endothelial-mesenchymal transformation of the cardiac valve.* Proc Natl Acad Sci U S A, 2011. 108(50): p. 19943-8.

37. Chen, C.S., et al., *Geometric control of cell life and death.* Science, 1997. 276(5317): p. 1425-8.

38. Nelson, C.M., et al., *Emergent patterns of growth controlled by multicellular form and mechanics.* Proc Natl Acad Sci U S A, 2005. 102(33): p. 11594-9.

39. Versaevel, M., T. Grevesse, and S. Gabriele, *Spatial coordination between cell and nuclear shape within micropatterned endothelial cells.* Nat Commun, 2012. 3: p. 671.

40. McWhorter, F.Y., et al., *Modulation of macrophage phenotype by cell shape.* Proc Natl Acad Sci U S A, 2013. 110(43): p. 17253-8.

41. McBeath, R., et al., *Cell shape, cytoskeletal tension, and RhoA regulate stem cell lineage commitment.* Dev Cell, 2004. 6(4): p. 483-95.

42. Kilian, K.A., et al., *Geometric cues for directing the differentiation of mesenchymal stem cells.* Proc Natl Acad Sci U S A, 2010. 107(11): p. 4872-7.

43. Parker, K.K., et al., *Directional control of lamellipodia extension by constraining cell shape and orienting cell tractional forces.* FASEB J, 2002. 16(10): p. 1195-204.

44. Bray, M.A., S.P. Sheehy, and K.K. Parker, *Sarcomere alignment is regulated by myocyte shape.* Cell Motil Cytoskeleton, 2008. 65(8): p. 641-51.

45. Alford, P.W., et al., *Vascular smooth muscle contractility depends on cell shape.* Integr Biol (Camb), 2011. 3(11): p. 1063-70.

46. Geisse, N.A., . *Micropatterning Approaches for Cardiac Biology*, in *Micro- and Nanoengineering of the Cell Microenvironment*. 2008.

47. Bray, M.A., et al., *Nuclear morphology and deformation in engineered cardiac myocytes and tissues.* Biomaterials, 2010. 31(19): p. 5143-50.

48. Tamura, K., et al., *Wound healing in the mitral valve.* J Heart Valve Dis, 2000. 9(1): p. 53-63.

49. Rabkin-Aikawa, E., et al., *Dynamic and reversible changes of interstitial cell phenotype during remodeling of cardiac valves.* J Heart Valve Dis, 2004. 13(5): p. 841-7.

50. Chester, A.H. and P.M. Taylor, *Molecular and functional characteristics of heart-valve interstitial cells.* Philos Trans R Soc Lond B Biol Sci, 2007. 362(1484): p. 1437-43.

51. Taylor, P.M., et al., *The cardiac valve interstitial cell.* Int J Biochem Cell Biol, 2003. 35(2): p. 113-8.

52. Desmouliere, A., et al., *Apoptosis during wound healing, fibrocontractive diseases and vascular wall injury.* Int J Biochem Cell Biol, 1997. 29(1): p. 19-30.

53. Schnittler, H.J., T. Schmandra, and D. Drenckhahn, *Correlation of endothelial vimentin content with hemodynamic parameters.* Histochem Cell Biol, 1998. 110(2): p. 161-7.

54. Bertipaglia, B., et al., *Cell characterization of porcine aortic valve and decellularized leaflets repopulated with aortic valve interstitial cells: the VESALIO Project (Vitalitate Exornatum Succedaneum Aorticum Labore Ingenioso Obtenibitur).* Ann Thorac Surg, 2003. 75(4): p. 1274-82.

55. Bairati, A. and S. DeBiasi, *Presence of a smooth muscle system in aortic valve leaflets.* Anat Embryol (Berl), 1981. 161(3): p. 329-40.

56. Cimini, M., K.A. Rogers, and D.R. Boughner, *Smoothelin-positive cells in human and porcine semilunar valves.* Histochem Cell Biol, 2003. 120(4): p. 307-17.

57. Blevins, T.L., et al., *Phenotypic characterization of isolated valvular interstitial cell subpopulations.* J Heart Valve Dis, 2006. 15(6): p. 815-22.

58. Win, Z., et al., *Smooth muscle architecture within cell-dense vascular tissues influences functional contractility.* Integr Biol (Camb), 2014. 6(12): p. 1201-10.

59. Chen, C.S., et al., *Micropatterned surfaces for control of cell shape, position, and function.* Biotechnol Prog, 1998. 14(3): p. 356-63.

60. Chen, C.S., et al., *Cell shape provides global control of focal adhesion assembly.* Biochem Biophys Res Commun, 2003. 307(2): p. 355-61.

61. Elineni, K.K. and N.D. Gallant, *Regulation of cell adhesion strength by peripheral focal adhesion distribution.* Biophys J, 2011. 101(12): p. 2903-11.

62. Feinberg, A.W., et al., *Muscular thin films for building actuators and powering devices.* Science, 2007. 317(5843): p. 1366-70.

APPENDIX

MATLAB CODE

```
%% This code is written for the stress calculation of the thin film assay.
%% The microscope images should be converted to binary images first and then
inserted here.
%% It will first remove the noises and gives a picture that just contains the
projected line of the thin film.
%% It then calculates the distance of the line from the baseline to give the
radius of the curvature.
%% Stress values are the obtained based on the radius of the curvature and
physical properties of the PDMS layer.
%%
%length analysis
clear;
close all;
clc;
 %number of frames
q=input('input the number of frames ');
[file,path]=uigetfile({'*.TIF';'*.tif';'*.bmp';'*.jpg';'*.*'});
filename = [path file];
f=71;g=126;
for i=1:q
%for i=1:f
%for i=72:g
im= imread(filename,i);
    %% noise removal by discarting elements with low number of pixels
    CC = bwconncomp(im);
    for j=1:CC.NumObjects
        if numel(CC.PixelIdxList{j})<200;

            im(CC.PixelIdxList{j})=0;
        end
    end


   % finding the index of rows
   % dist(j) will contain distance from bottom in column j
    S=0;I=0;
    for j=1:size(im,2)
        t_row = max(find(im(:,j)));
        if ~isempty(t_row)
            %dist(j)=size(im,1)-t_row;
            dist(j)=t_row;
            S=S+dist(j);I=I+1;
        else
             dist(j)=-1;
        end


    end
 %the length are in micrometers
 %10000 um/#pixels measured in imagej (when scale is 1 cm)
 % "ps" represents pixel size and may vary for each experiment based on the
microscope set up
```

```
 %(It is recommended to calculate pixel size for each experiment
%ps=1.014;
ps=1.025;
im1=imshow(im);
avg_pdist(i)=S/I;
avg_dist(i)=ps.*avg_pdist(i);

end
% disp(avg_dist)
L=size(im,1)*ps;%x=L-avg_dist;
x=avg_dist;
% stress calculations
E=1.5; %MPa pdms elastic modulus
t=30; %um pdms thickness
h=5; %um 2D myocardium thickness
nu=.49; %poisson's ratio of pdms
%R is the radius of curvature for each frame of the video
%%
x=transpose(x);r=zeros(q,1);stress=zeros(q,1);
%x=transpose(x);r=zeros(f,1);stress=zeros(f,1);
%x=transpose(x);r=zeros(g,1);stress=zeros(g,1);


for i=1:q
%for i=1:f
%for i=72:g
    if x(i)<L && x(i)>2*L/pi
    r(i)=fzero(@(R)radius(x(i),R,L),50);
    else if x(i)<2*L/pi
    r(i)=x(i);
        end
    end
     stress(i)=(E*(t^3))./(6.*r(i)*(1-nu)*(h^2)*(1+t/h));
    % stress(i)=70.13/r(i);
end
%%
% stress=transpose(stress);
% time=0:15:((15*q)-15);
% figure(1)
% plot(time,stress,'.')
% xlabel('time (s)')
% ylabel('stress (MPa)')
%%
%stress
%% Stress values are neglected before adding the ET-1 at 2.5min=12*15sec
finalstress=stress(12:q)-stress(12);
normalstress=1e+3*finalstress/L;
time=transpose([12*15:15:q*15]);
figure(2)

%% The stress values are normalized with the length of the picture(MPA/mm)

normalstress=1e+3*finalstress/L
 % figure(2)
 %plot(time,stress)
 plot(time,finalstress)
```